405 803

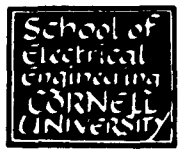

CORNELL UNIVERSITY

SCHOOL OF ELECTRICAL ENGINEERING

RESEARCH REPORT EE 538

Noise near the Carrier in Microwave Oscillators

C. H. Mosher

1 October 1962

MICROWAVE NOISE, Technical Report No. 10

[Contract No. DA36-039-sc-87368]

School of Electrical Engineering
CORNELL UNIVERSITY
Ithaca, New York

RESEARCH REPORT EE 538

NOISE NEAR THE CARRIER IN MICROWAVE OSCILLATORS

C. H. Mosher

MICROWAVE NOISE

Technical Report No. 10 1 October 1962

Published under U. S. Signal Corps Contract No. DA36-039-sc-87368
U. S. Army Signal Research and Development Laboratory, Fort Monmouth, N. J.

CONTENTS

ABSTRACT

This study of noise near the carrier in microwave oscillators was primarily an experimental survey of typical tubes. The noise in the oscillator's output was detected as equivalent modulation by a receiver similar to those used in noise-measuring test sets available commercially. The signals of interest were fed into a spectrum analyzer which resolved them into self- and cross-spectra, the frequency range from 14 c/s to 34 kc/s being resolved into 25 bands of about 1/2 octave each. The cross spectra were derived from measurements of the self-spectra of linear combinations of the signals, with wide-band phase shifters having been used to permit observation of the imaginary components of the cross spectra.

It was found that amplitude noise in the outputs of the oscillators tested (VA203, V217, VA161, QK610, 357H) was too small to be observable with a receiver of this type, and that internally generated low-frequency beam-current fluctuations were not significant in producing frequency noise. The frequency-noise spectra observed were consistent with spectra that might be expected from theory, if independent ions were assumed in the interaction region.

INTRODUCTION

The objective of this study is to obtain insight into those mechanisms peculiar to the production of noise sidebands near the carrier in voltage-tunable microwave oscillators. Since the nonlinear properties of many types of microwave oscillators are extremely difficult to analyze theoretically, this study is necessarily an experimental survey primarily, except when the experimental results suggest that useful results in closed form can be obtained easily from simple models.

Here we have termed "near" sidebands those which are most easily observed as apparent modulations rather than as more or less distinct sidebands on each side of the carrier. The measuring apparatus therefore consists of two relatively distinct sections: the receiver, which detects the equivalent noise modulations in the oscillator's output, and the spectrum analyzer, which measures the spectra of these modulations in the frequency domain.

EXPERIMENTAL EQUIPMENT AND METHODS

THE RECEIVER

The receiver is shown in simplified block form in Figure 1. The part of the receiver that detects the equivalent amplitude-modulation noise is rather conventional, having a mixer crystal with a relatively large local-oscillator injection and relatively small "signal" applied, and an intermediate-frequency amplifier and conventional envelope detector. If a crystal diode detector were used at the signal frequency, the low-frequency

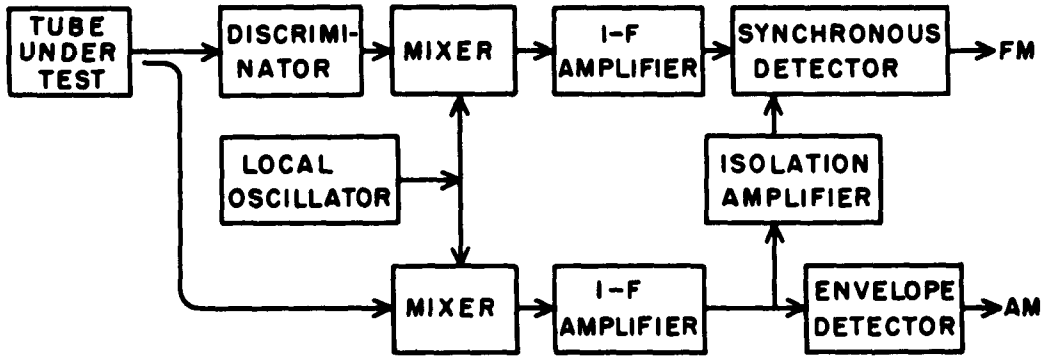

Figure 1. Block Diagram of Receiver.

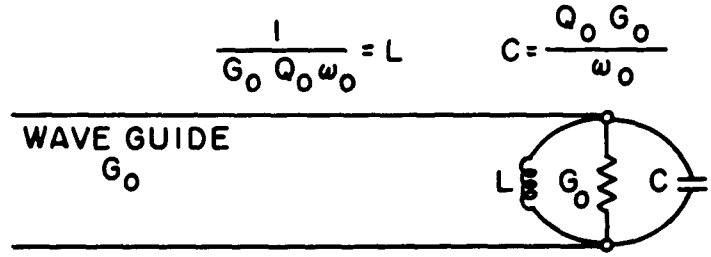

Figure 2. Equivalent Circuit of Discriminator Cavity.

spurious signals in the post-amplification that would be required would be combined additively, while a superheterodyne receiver permits much amplification before the signals must be handled in low-pass form, so that the flicker noise in the mixer crystal and intermediate-frequency amplifier appear only as relatively small intermodulation products. Even so, it is these intermodulation products with the carrier in these elements that limits the sensitivity.

The discriminator was at the signal frequency before the mixer rather than after the mixer, where the frequency modulation in the local oscillator would be combined additively with that of the tube under test. The type of discriminator used here is similar to that used in commercially available noise-measuring test sets.* The discriminator used a magic-T as a 3-db directional coupler to observe the reflection coefficient of a critically coupled cavity. If the cavity is represented schematically as in Figure 2, where everything is normalized against the wave-guide characteristic admittance, one then finds that at the appropriate virtual detuned short plane, the current reflection coefficient is

$$k = \frac{Y - G_o}{Y + G_o} = \frac{j \frac{\omega Q_o}{\omega_o} - j \frac{Q_o \omega_o}{\omega}}{2 + j \frac{\omega Q_o}{\omega_o} - j \frac{Q_o \omega_o}{\omega}} \quad ;$$

*We would like to thank Bruce Morley of Varian Associates for his generosity in discussing the circuit with us, as it is more easily adjusted and more sensitive than the circuit we were using initially.

or defining

$$\delta = \frac{Q_o}{2}\left(\frac{\omega}{\omega_o} - \frac{\omega_o}{\omega}\right) \approx Q_o \frac{\Delta\omega}{\omega_o} \approx Q_o \frac{\Delta f}{f_o} \quad ,$$

where $\Delta f = f - f_o$; then

$$k = \frac{j\delta}{1 + j\delta} = \frac{\delta^2}{1 + \delta^2} + \frac{j\delta}{1 + \delta^2} \quad .$$

Thus it is apparent that for small δ this arrangement can be used to convert frequency modulation to double-sideband, suppressed-carrier amplitude modulation, where the frequency signal can be recovered later upon synchronous detection against a carrier of appropriate phase. By using a common local oscillator for both mixers, relative phase can be preserved through the mixing process. Note that the carrier was effectively removed from the receiver handling the sidebands representing the frequency modulation, so that intermodulation products occurring here were doubly small and could be completely neglected. An automatic frequency control on the tube under test was provided to maintain this condition, which was relatively uncritical in spite of the high gains that were sometimes used in the receiver.

Some tubes were so noisy that the high sensitivity of the superheterodyne receivers was not needed. In this case, the termination used with the magic-T was replaced with an adjustable short circuit and the outgoing signals in the two side arms fed to square-law crystal detectors. In this case, we can express the two signals, with suitable short-circuit adjustment, as follows:

$$k_1 = \frac{\delta}{1+\delta^2} + \frac{j\delta}{1+\delta^2} + j \quad ,$$

$$|k_1|^2 = \frac{\delta^4 + (1+\delta+\delta^2)^2}{(1+\delta^2)^2} = \frac{1+2\delta+3\delta^2+2\delta^3+2\delta^4}{(1+\delta^2)^2}$$

$$= 1 + \frac{2\delta+\delta^2+2\delta^3+\delta^4}{(1+\delta^2)^2} = 1 + \frac{2\delta+\delta^2}{1+\delta^2} \quad ;$$

$$k_2 = \frac{\delta^2}{1+\delta^2} + \frac{j\delta}{1+\delta^2} - j$$

$$|k_2|^2 = \frac{\delta^4 + (1-\delta+\delta^2)^2}{(1+\delta^2)^2} = \frac{1-2\delta+3\delta^2-2\delta^3+2\delta^4}{(1+\delta^2)^2}$$

$$= 1 + \frac{-2\delta+\delta^2-2\delta^3+\delta^4}{(1+\delta^2)^2} = 1 + \frac{-2\delta+\delta^2}{1+\delta^2} \quad .$$

If we then take the difference of these detected signals as the output,

$$\text{output} = \left|k_1^2\right| - \left|k_2\right|^2 = \frac{4\delta}{1+\delta^2} \quad .$$

This type of discriminator was very simple to set up and adjust, but had the disadvantage that with available values of Q_o, tubes which produced relatively little frequency modulation, such as some reflex klystrons, produced so little output from this discriminator that flicker noise in the crystal detectors limited the sensitivity.

Synchronous detection is, of course, merely sampling the signal periodically as determined by the phase of the reference voltage. Several vacuum-tube circuits were tried, but they were found unstable in their symmetry and isolation, therefore the circuit shown in Figure 3 was used. If care is taken in symmetry of component location and lead dress, the circuit is found to be quite stable and to have excellent isolation between the sideband and carrier inputs and to have excellent amplitude modulation rejection from the carrier input. Although we did not do so, it would be sound procedure to mount both intermediate-frequency amplifiers, the isolation amplifier, and the synchronous detector on a common chassis, with appropriate shielding and decoupling, in order to avoid interconnecting cables, the quality of which can be troublesome as far as shielding, ground loops, and bandwidth are concerned.

Although the channel that processes the output of the discriminator is required to process only small signals, it must have good linearity. As it is convenient to monitor the output of this intermediate-frequency amplifier in tuning up the discriminator cavity, care must be taken that the detector used for this purpose keeps the operation of this amplifier from becoming nonlinear. It was found that a suitably designed "infinite-impedance" detector using a 12AU7, with the other half of the tube being used for drift cancellation, was satisfactory. It is of course desirable that this amplifier have the same delay (phase-versus-frequency) characteristic as the other cascaded amplifiers, so that drift in the local-oscillator frequency would not disturb the phase relations at the synchronous detector, but this is easily accomplished and is not critical in any case. The synchronous detector unit has a discriminator to provide automatic frequency

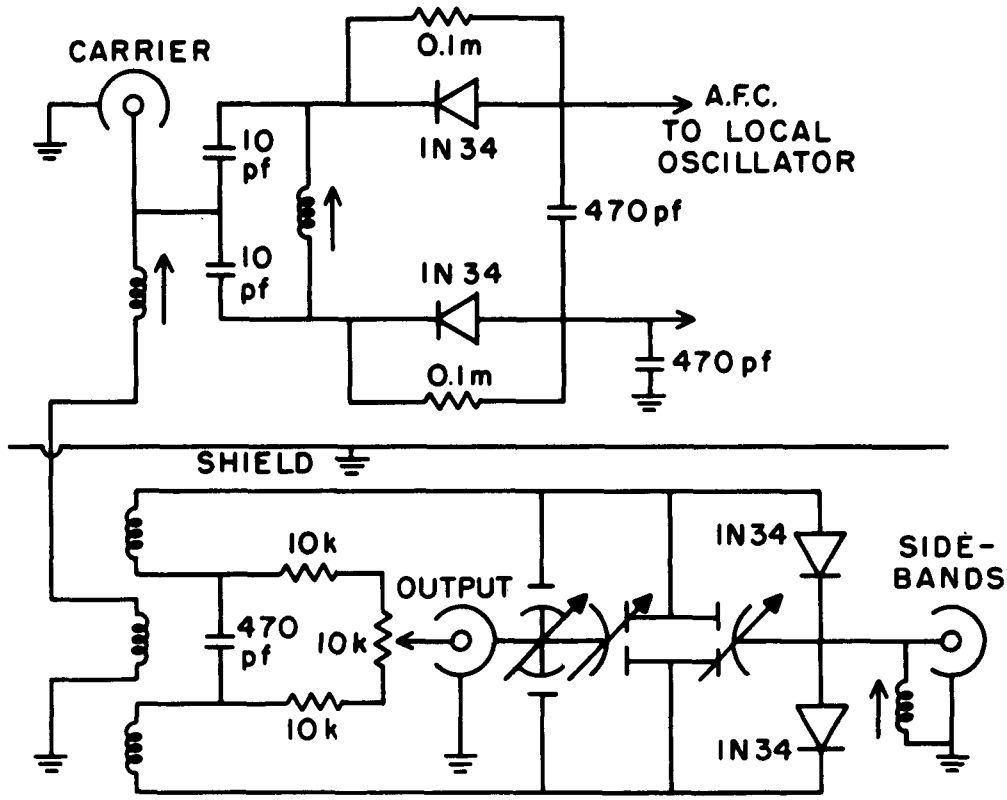

Figure 3. Schematic of Synchronous Detector.

control for the local oscillator to control this phase relationship in addition to other considerations to be discussed below.

The receiver that drives the amplitude-modulation detector is rather critical, as the carrier is present throughout, and intermodulation can occur with spurious signals at any point. The intermediate-frequency amplifier was two stages of 6AG7's with the inputs matched for best thermal noise figure, the outputs matched for best power output to minimize nonlinearities which could provide intermodulation mechanisms, and with a large amount of degeneration introduced by not bypassing the cathode bias resistors at low

frequencies to minimize the amplitude of any low-frequency signals present from causes such as flicker noise. The grids were operated at 45 volts positive with respect to the negative terminal of the plate supply, this bias being derived from heavily decoupled dry-cell batteries; direct current was used on the heaters; and the supply was well regulated with additional passive filtering. Under all conditions the observed amplitude-modulation noise, when it could be observed at all, seemed to be constant, suggesting that the primary source was flicker noise in the mixer crystal. Various mixer crystals did not seem to differ appreciably in this respect. Several levels of local-oscillator injection and several levels of signal at the mixer were tried, and the observed amplitude modulation index was essentially constant.

One difficulty, the importance of which was initially underestimated, was the problem of slope detection of frequency modulation in this intermediate-frequency amplifier. Not only did the frequency modulation of the tube under test appear in this way, but also that of the local oscillator. Thus it is desirable that the local oscillator contribute very little frequency modulation. It was found that it was very difficult to prevent coherent spurious signal from being injected in this way; for although the local oscillator was a reflex klystron with very low frequency noise, there was enough frequency modulation in its output because of external magnetic fields varying at 60 cps that appreciable 120-cps signals would be produced in the amplitude modulation output of the receiver from this source. The half-power bandwidth of the intermediate-frequency amplifier feeding the amplitude-modulation detector was over one megacycle, being mostly limited by interconnecting cables, but it was not designed so that it could be stagger tuned to be flat to second or higher order in its frequency response. Such

a high-order stagger would be highly desirable if it could be aligned in practice, but it is not clear how this could be done with the necessary precision. The inclusion of an automatic frequency-control feedback loop on the local oscillator helps to control the linear slope detection, but the nonlinear products of such slope detection are a nonlinear change of variables, which cannot be corrected for in the data.

With the exception of the intermediate-frequency amplifier for the double-sideband, suppressed-carrier signal from the discriminator output, it was found that spurious signals from power supply sources were large enough that extreme measures had to be taken merely to reduce them to the point where they did not prevent measurements completely by overloading the apparatus at some point. It was found that all high voltages had to be extremely well regulated and be provided with additional passive filtering between the regulators and the circuit of use. It was found that nothing except battery-supplied direct current could be used on the heater of the tube under test, under any conditions, and that amounts of hum or hash in supplies that were rectified, filtered, regulated, and filtered again were excessive in their effect on the tubes tested, although not observable in the supply output. Among other things, a high-voltage power supply with only 120 μv of spurious signal at the regulator output (mostly 120 cps ripple) before the passive filters was developed. This was found to be reasonably satisfactory, but better supplies are needed, which require voltage references with lower noise levels that are not currently available.

SPECTRUM ANALYZER

The spectrum analyzer takes the equivalent noise modulations, and a signal derived from the beam current of the tube under test via a load

resistor and a Tektronix 122 preamplifier, and estimates their spectra in frequency. Signals are of course brought to the appropriate amplitude by calibrated attenuators and amplifiers. They are then passed through band-pass filters, and the "power" or mean-square amplitude for each band is measured with a square-law detector. If two signals are linearly independent, then the power of the sum of the signals is the sum of their powers; if they are completely linearly dependent on each other, their amplitudes could add or subtract perfectly, giving a power somewhere between zero and twice the sum of the powers of the two signals taken independently. Thus this type of correlation can be measured by merely measuring the power of the two signals added together and comparing the sum with their individual powers.

However, suppose there were a cosine signal and sine signal, then one completely determines the other, but now the signals are linearly independent. This type of situation corresponds to a non-zero value of the imaginary component of the frequency-domain cross spectrum and can be measured by first applying appropriate phase shifts to the signals and proceeding as above. For this purpose, sets of phase shifters whose phase shift differs by approximately 90° over a three-octave band were constructed. As the filters which determine the band whose power is to be measured are only about one-half an octave wide, one phase shifter design suffices for about six different filters, and only four different phase shifter sets had to be constructed. The design of such phase shifters is a well-known circuit-theory problem, as they are commonly used in the generation of single-sideband, suppressed-carrier signals.

The filters used were active RC filters using small economical

operational amplifiers with feed-back loops, the positive feed-back loop being similar to that used in Hewlett-Packard audio oscillators. Three of these were cascaded in a third-order Butterworth stagger to give a set of contiguous one-half octave band-pass filters that were tuned by a switch, spanning the range from 14 cps to 34 kc/s, in 25 bands. The sharpness of each resonance is adjusted by its negative feed-back loop. There are a number of filter sets available commercially which can be used if desired.

The detector had to be very close to true square law and yet be relatively free from drift. As the signals being measured would at times be decidedly nonstationary for short intervals of time, the detector had to be square law well above the "normal" signal levels and could not evidence any transient or permanent changes in its properties after an overload. The circuit shown in Figure 4 was developed, which owed its low drift to the use of selected Western Electric 420A's in all critical sockets, and its tolerance of overloads to the use of symmetrical "infinite-impedance" detectors. Low-leakage capacitors with the cases used as guard rings were used in all critical circuits. The detector drove an Esterline Angus recording meter, which made the record of the data, the various signals of interest being automatically selected in sequence by a stepping relay. The detector incorporates an average time of about 2 seconds.

CALIBRATION

The calibration procedures for the apparatus are relatively straightforward. The frequency-modulation sensitivity of the receiver is easily calibrated by applying sine-wave frequency modulation to the tube under test of such a magnitude that the modulation index is 2.405, making the carrier

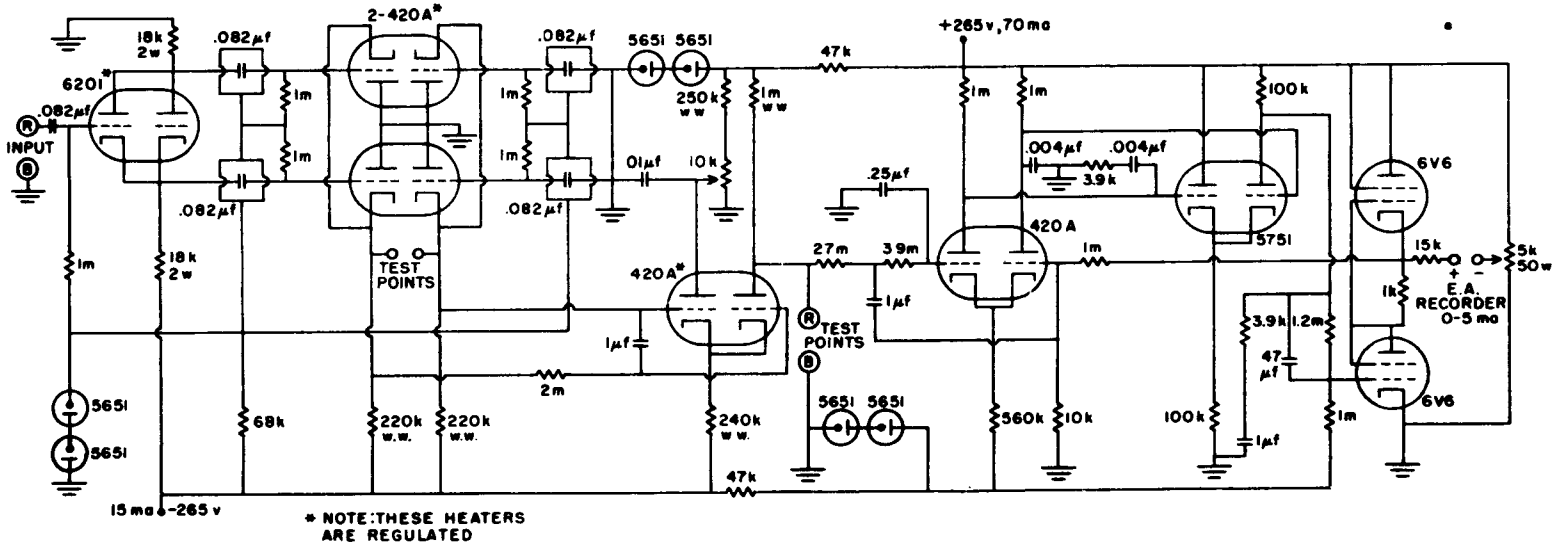

Figure 4. Schematic of Square-Law Detector

zero. A Polarad SA-84 spectrum analyzer was used to observe the carrier magnitude, and the modulating signal was a 33 1/3 kc/s sine wave obtained by triggering a multivibrator on the third subharmonic of a 100-kc/s crystal and filtering the waveform to obtain a good sine wave. An accurately calibrated attenuator was used to drop the modulation index to whatever magnitude was most convenient for the receiver calibration. A deviation of about one order of magnitude above the total mean-square deviation of the tube under test was appropriate, since an average absolute meter such as a Hewlett-Packard 400 D will then not indicate the noise. Care should be taken that the intermediate-frequency amplifier is not overloaded.

Since it may be desirable to operate the mixer in the amplitude-modulation receiver under large-signal conditions to obtain the maximum sensitivity to the amplitude modulation originating in the tube under test, it is necessary to calibrate the amplitude-modulation receiver with a known standard signal at the "signal" frequency, so that the nonlinearity of the mixer is included in the calibration. Such a test signal can be obtained with a ferrite modulator, where the calibration is obtained from a crystal detector at the signal frequency, which is in turn calibrated by assuming that it becomes square law at very small signals and by using square-wave modulation to measure the carrier level.

Of course all amplifiers, filters, attenuators, and phase shifters must be calibrated in gain and phase, but this is easily done as they operate at audio and near audio frequencies. Provision was included to check periodically the zero and the calibration of the square-law detector automatically, the reference signal for this purpose being derived from a one-kilocycle square wave clipped by a Zener diode.

DATA REDUCTION

If we are dealing with a set of voltages or signals, which we consider as the basis of a linear vector space, and which we write as a column vector ξ with its components expressed in the frequency domain, we can also visualize the spectra of the set of signals by considering the "power" or mean-square value of a combination of these voltages, $E = a^{\dagger}\xi$, as a Hermitian form, $P = a^{\dagger}S\,a$, where

$$[S] = \begin{bmatrix} S_{11} & S_{12} \cdots S_{1n} \\ S_{12}^{*} \cdots\cdots\cdots \\ \cdots\cdots\cdots S_{nn} \end{bmatrix} \quad ;$$

and where the dagger ($\dagger$) is used to indicate the conjugate transpose, and properly speaking, the "power" is per unit bandwidth, just as in a spectrum defined for a single signal only. The asterisk indicates the complex conjugate of a number.

The elements of the spectrum matrix S can be found by measuring a number of ordinary power spectra. If $a^{\dagger}$ is $(1, 0, \ldots, 0)$, then P is S_{11} for example; while if $a^{\dagger}$ is $(1, 1, 0, \ldots, 0)$, then P is $S_{11} + S_{22} + 2\,(\text{real } S_{12})$; and if $a^{\dagger}$ is $(1, j, 0, \ldots, 0)$, then P is $S_{11} + S_{22} + 2\,(\text{imaginary } S_{12})$. The measurement procedure is simply to take the signals two at a time and to measure these ordinary power spectra as has been described above. As in any measurement of power spectra, we will get only an approximation to $P(\omega)$, and will have to keep in mind at all times the degree of approximation actually obtained. In particular, arbitrary accuracy and fine resolution in ω would require long averaging time, which is not available to us.

This expression of the spectra as a Hermitian form in the frequency domain lends itself readily to changes of variables by linear time-independent operators, which in the frequency domain simply become matrix multiplication with the elements being functions of frequency. As an example, let us consider a linear frequency-independent change of variable such as would be produced by some artificial constraint on a device necessary to permit some measurement, such as inserting a load resistor to sense beam current in a reflex klystron. Such a constraint produces a linear combining of the small signals and the coefficients of this combination must be measured. This is readily done by deliberately inserting a known coherent signal. We can thus execute the known change of variable to a new basis set D:

$$\xi = F D \quad ;$$

but

$$E = a^{\dagger}\xi = a^{\dagger}F D = b^{\dagger}D \quad ,$$

so

$$b^{\dagger} = a^{\dagger}F \, , \qquad a^{\dagger} = b^{\dagger}F^{-1} \, , \qquad a = F^{-1\dagger} b \quad .$$

Expressed in terms of the new basis set, the power is

$$P = b^{\dagger} T b = b^{\dagger} F^{-1} S F^{-1\dagger} b \quad ;$$

therefore

$$T = F^{-1} S F^{-1\dagger} \quad .$$

By matrix manipulations of this type the spectra can be referred from one part of the system to another and systematic errors removed.

A compromise between accuracy, resolution in frequency, and averaging time must be made. Resolution and accuracy are limited and cannot be improved indefinitely in an experimental device. In fact, we must proceed under the assumption that any quantity describing the performance of the device has zero as its time average, so that any phenomenon of interest to us is nonstationary, is dependent on initial conditions and past history, and has a useful time average only in a semi-convergent sense. We might hope that this semi-convergent time average approximates what a population average would be if a population were available. Thus the limits of resolution and accuracy resulting from theoretical considerations are appreciable, although any given short-time average may appear to converge satisfactorily.

One change of variable that facilitates visualizing the results is a diagonal transformation, which makes the diagonal elements of T be unity in value. We will have occasion to use this to display the cross spectra in dimensionless form, and the notation used will be

$$[\Gamma] = \begin{bmatrix} 1, & \Gamma_{12} \cdots & \Gamma_{1n} \\ \Gamma^*_{12}, & 1 \quad \Gamma_{ij} \cdots & \vdots \\ \vdots & & \\ \Gamma^*_{1n}, & \cdots & 1 \end{bmatrix} .$$

EXPERIMENTAL RESULTS

AMPLITUDE MODULATION NOISE

As has already been mentioned in the discussion of the apparatus, considerable difficulty was experience in attempting to measure the ampli-

tude-modulation noise of the various tubes. At no time was a level of amplitude modulation observed that was appreciably above that originating in the receiver itself, which was the slope-detected frequency modulation and the intermodulation of flicker noise in the mixer crystal with the signal carrier. In the cases where the noise frequency deviation was large, the FM and AM noise signals could be displayed on an oscilloscope, yielding a display like that shown in Figure 5 in which the vertical co-ordinate is amplitude and the horizontal co-ordinate, frequency. This is merely the frequency response of the intermediate-frequency amplifier as scanned by the frequency noise of the tube under test. Thus, while, on each of the tubes tested, the amplitude noise was at least checked, and in several cases quantitatively measured, no amplitude noise actually originating in the tube under test was ever detected, except in reflex klystrons operated on the side of a mode.

TUBES TESTED

Each of the tubes tested was tested as close to the manufacturer's

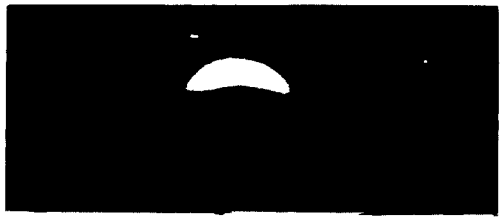

Figure 5. Lissajous Figure of Amplitude versus Frequency for VA161 No. 1148.

recommended operating conditions as possible and in some cases under more nearly optimum operating conditions.

Table I. identifies the frequency bands in which the spectra were measured.

TABLE I.

Filter Bands Used

cps	cps	cps	cps	kc/s	kc/s	kc/s	kc/s
14	20.7*	100	142	.91	1.28	7.95	10.8
20.2	28.8	137	196	1.24	1.72	10.8	14.6
27.5	39.4	191	270	1.67	2.34	14.6	19.5
38.5	54.5	261	366	2.31	3.22	19.8	26.0
53.0	75.0	343	480	3.18	4.40	26.4	33.8**
72	102	474	660	4.35	6.05		
		645	915	5.95	8.25		

* Lowest band
** Highest band

VA203B Tube: This relatively inexpensive reflex klystron was used for the initial development and adjustment of the apparatus. Like most of the tubes tested, it would exhibit very nonstationary spectra until it had been operated many hours a day for several days. Even under the best conditions, the noise in the lower four bands was so erratic as to be meaningless, and it is missing in Figure 6. Although a significantly non-zero correlation between frequency and beam current was observed, it was a negligible fraction of the total mean-square deviation. In the figures, the frequency noise spectra are expressed in mean-square deviation in $(\text{cycles per second})^2$ per band (of about $\frac{1}{2}$ octave). The beam noise is in mean-square nanoamperes per band, and the ion current collected by the reflector at the operating conditions is 10^{-7} amperes.

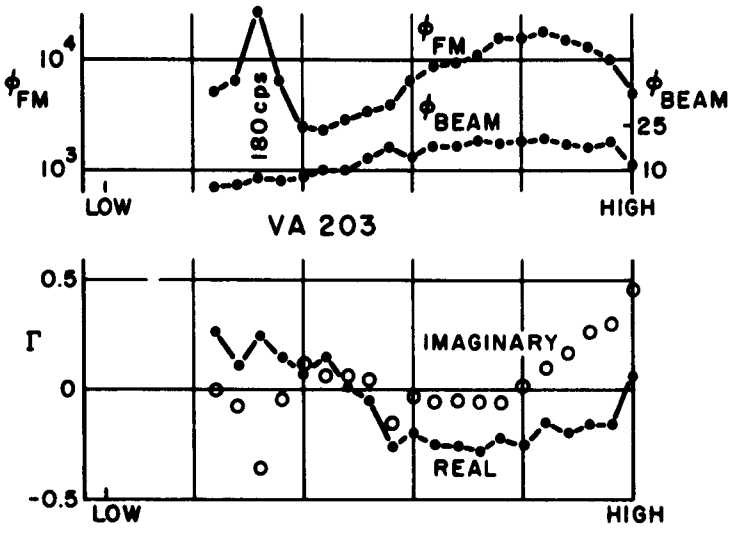

Figure 6. Spectra of VA203.

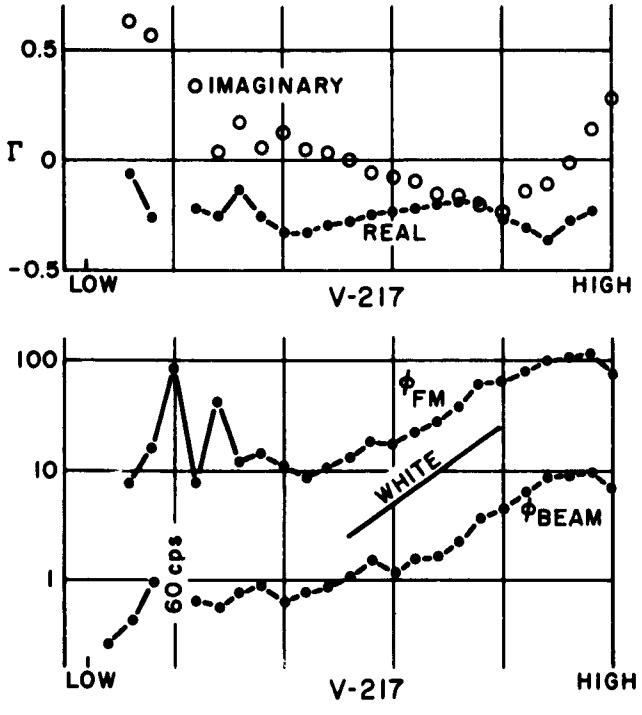

Figure 7. Spectra of V-217.

V217 Tube: This is a rugged ceramic and metal reflex klystron, and because of its low noise level, it was necessary to mount the entire apparatus on coil springs, so that its microphony would not override the low noise output. It was also necessary to add about 10^{-3} gauss of vertical magnetic field at 60 cps to cancel the effect of the 60-cps fields in the environment and to avoid overloading the apparatus. Again the correlation was small. The ion current collected by the reflector was 1.25×10^{-8} amperes. The spectra of V217 are shown in Figure 7.

VA161 No. 1149 Tube: This is a backward-wave oscillator that requires a helix voltage of about 200 volts to operate at 9 Gc/s. Its spectra when thoroughly warmed up with free air convection cooling are shown in Figure 8. With restriction of the air flow, it generated coherent frequency modulation. The large magnitude of the beam self-spectrum was due to noise in the Zener diodes which regulated the anode supply of the gun and were not adequately decoupled. Even with this high noise level in the power supply, the correlation is still small enough that a reliable estimate could be made of the net spectrum if this modulating power-supply signal were removed. Both VA161's tested tended to develop leakage from the various leads to the envelope, and tests had to be terminated on this tube when the leakage could not be burned out with a Tesla coil.

VA161 No. 1148 Tube: The spectra of this tube with free air convection cooling is shown in Figure 9. The higher level in the frequency noise spectra did not appear until about 20 minutes after the tube had been in operation. The correlation between beam current and frequency is somewhat smaller than in Tube No. 1149 although the Zener noise was still applied to the tube. In both these cases, the collector, which was actually an ion trap, was biased

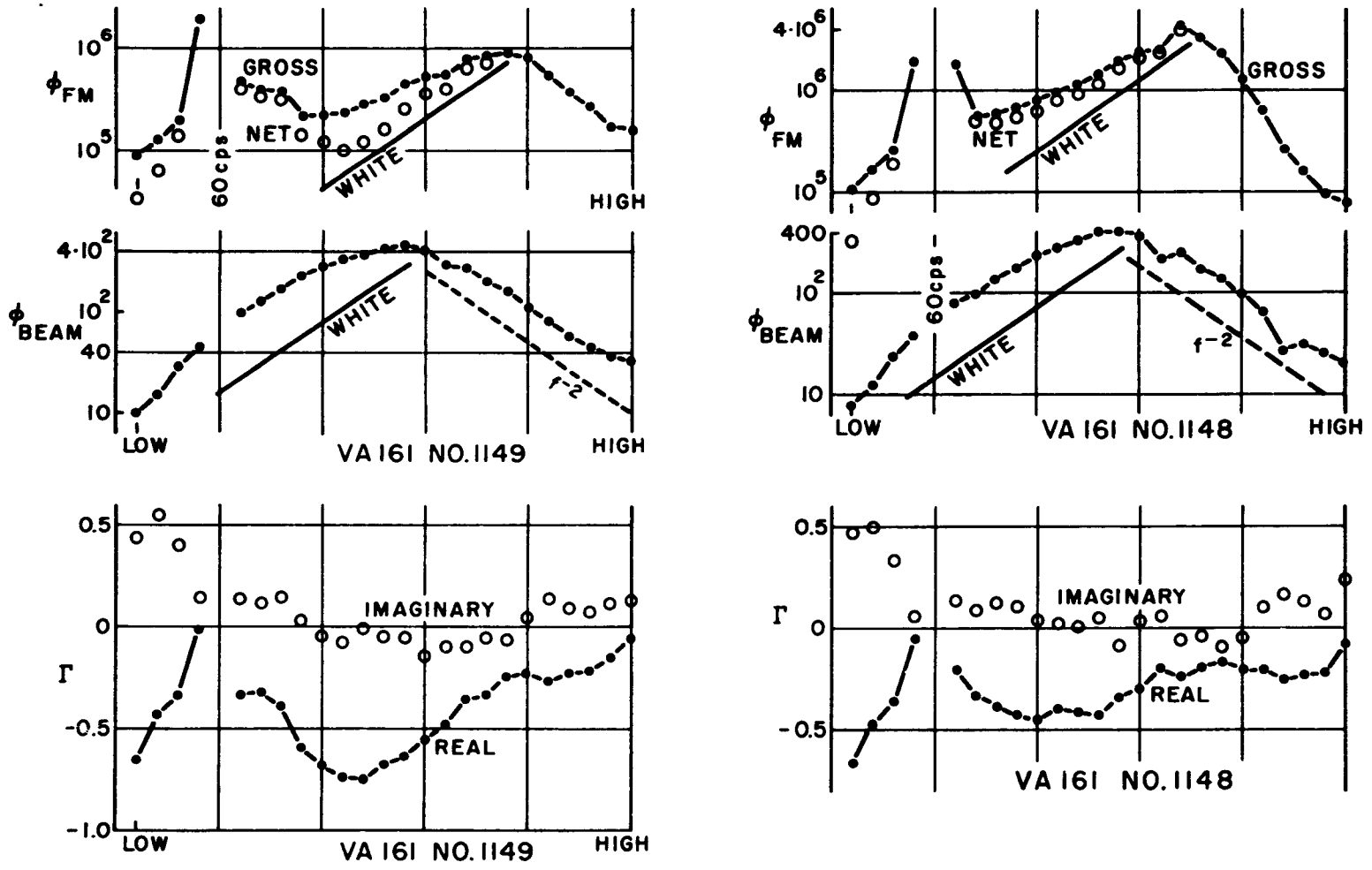

Figures 8, 9. Spectra of VA161 No. 1149 and No. 1148. (Without adequate decoupling of Zener diodes in gun anode supply, and with collector bias not optimum).

with the voltage drop of the intercepted beam current through 100,000 ohms, which may not have been adequate for full ion trapping. This, together with the sudden and dramatic rise in the frequency noise during warmup, suggested that better performance could be obtained from this particular tube.

This tube was later measured under identical conditions except that forced air cooling with controllable temperature at the air inlet was provided, with the air passing in and out of the housing through bolt clearance holes. The ion trap was biased with dry-cell batteries at about 70 volts negative with respect to the helix, at which point additional bias produced no further decrease in frequency noise, and the Zener diodes were thoroughly decoupled. At high temperatures this tube also produced coherent frequency modulation, while at low temperatures a relaxation oscillation in frequency and beam current occurred, in the form of a jump every second or two of several hundred kilocycles for about 10 ms and a return to the original frequency. In between these temperature limits the noise level increased rapidly with air temperature, at the rate of about one db for every two degrees Centigrade (estimated). The relative frequency-noise spectrum is shown in Figure 10. Here measurements on the lower bands are not shown because they had to be terminated when the regions of operating temperature that produced coherent frequency modulations approached each other. The beam noise was very nonstationary, even after forty hours of continuous operation, but the dimensionless correlation was estimated at not above 0.2 in magnitude. The figure shows only a relative-frequency noise spectrum, since the tube became inoperable before the apparatus could be calibrated. Under the operating conditions used in Figure 9, the ion trap collected 4×10^{-7} amperes of ions when it was run negative with respect to the cathode.

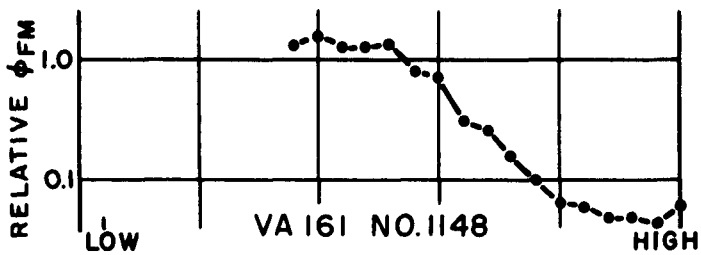

Figure 10. Relative Frequency Noise Spectrum of VA161 No. 1148 under Ideal Conditions.

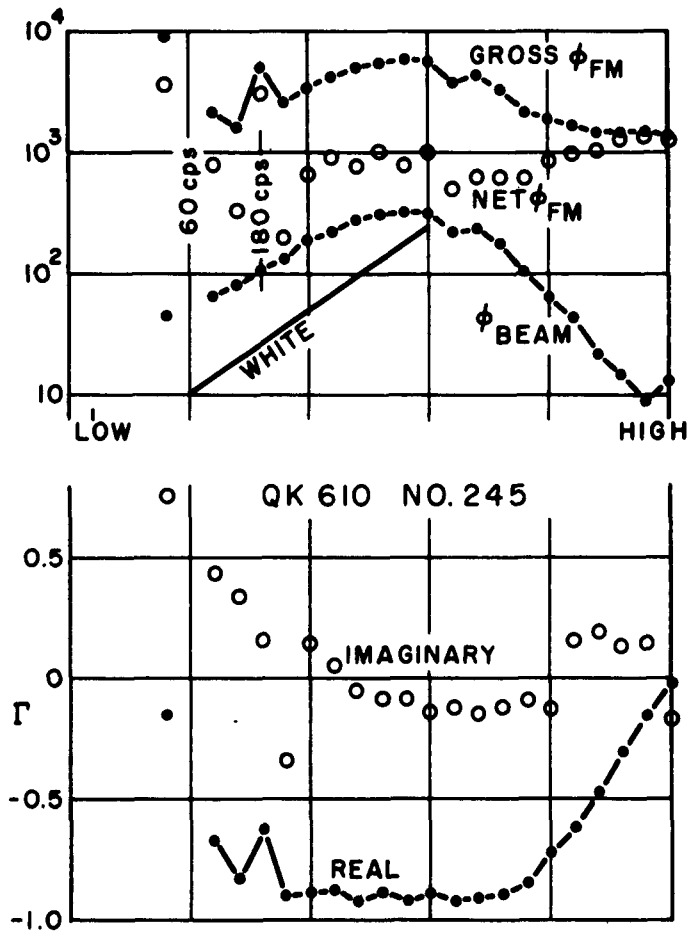

Figure 11. Spectra of QK610 No. 245. (With inadequate decoupling of Zener diodes in gun anode supply.)

QK610 No. 245 Tube: This is a backward-wave oscillator requiring about 500 volts on the helix to operate at 9 Gc/s. It has provision for forced air cooling, and was found to have stationary spectra, shown in Figure 11, and to reach steady-state operating conditions relatively quickly. Note the relatively low magnitude of the frequency noise, in spite of the beam noise resulting from the poorly decoupled Zener diodes; also the relatively high value of the correlation, so that an estimate of the net frequency noise actually produced by the tube would be relatively inaccurate.

This tube was relatively microphonic, this microphony being emphasized by the low amount of frequency noise. The microphony appeared in the beam current also, but not in sufficient magnitude to explain the frequency modulation by this mechanism alone. The low-frequency bands were not included here because of coherent signals resulting from the magnetic field of the cooling blower, which was only 18 in. away.

Because of the high correlation between frequency and beam current, the beam-current fluctuations being due to the Zener diodes as before, the measurements were repeated with this source of a spurious signal removed. The cooling air was also provided from a remote blower via fiberglass hose. The spectrum observed under these conditions is plotted in Figure 12; here the beam current noise was so small as to be unmeasureable, and correlation was observed only for coherent power supply signals. The droop at the low-frequency end was due to noise cancellation by the feed-back loop which provided automatic frequency control and had to be made rather rigid to control microphony.

This tube would produce coherent spurious frequency modulation if operated in an unmodified state, in the form of a sawtooth of about 400 cps,

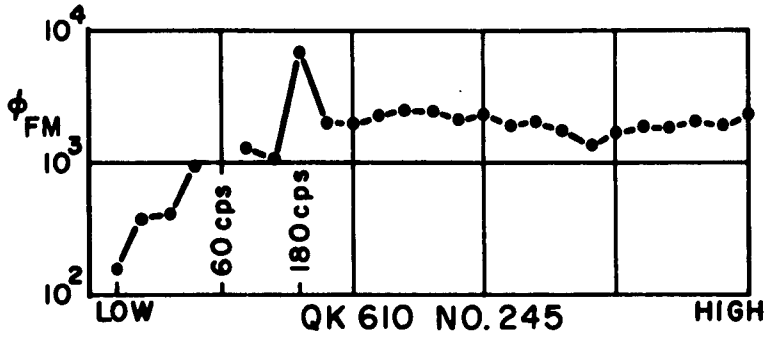

Figure 12. Spectrum of QK610 No. 245 under Optimum Conditions.

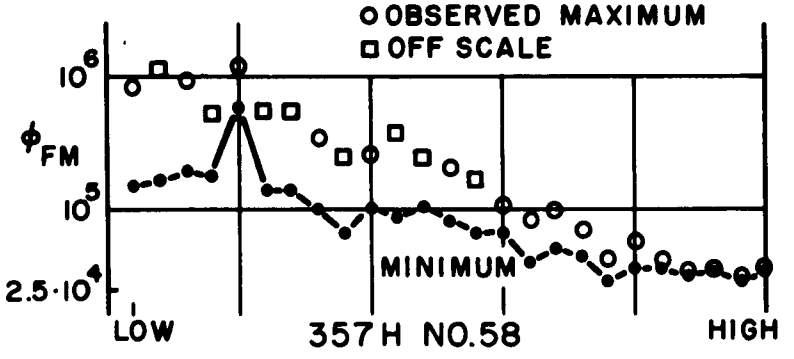

Figure 13. Frequency Noise Spectrum of 357 No. 58.

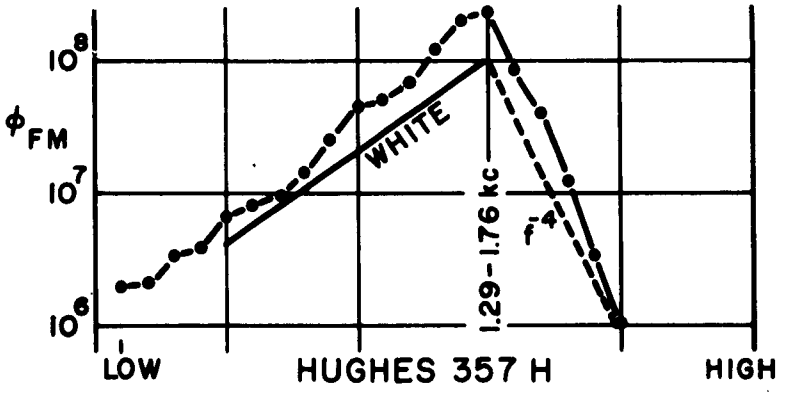

Figure 14. Frequency Modulation Noise of a Hughes 357H. (Abnormal Behavior)

or a nearly sinusoidal waveform at about 7 kc/s, where if by some means these were removed, there remained a sharp peak in the noise spectrum at 7 kc/s. All these phenomena were eliminated by a slight concentration of the magnetic field at the cathode end of the tube by means of a pole piece. Several other tube types could not be tested at all because of such coherent spurious modulations. At no time did the external environment contribute a magnetic field of more than 3 gauss.

The QK610 evidenced a pair of coherent sidebands about 2 Mc/s on each side of the carrier, down about 45 db ; it also produced a sideband about 22 Mc/s lower in frequency than the carrier, about 40 db below the carrier in amplitude, as well as other sidebands which might have originated in the spectrum analyzer.

357H No. 58 tube: This backward-wave oscillator requires a helix voltage of about 500 volts for operation at 9 Gc/s. It is meant to be cooled by means of conduction through its mechanical mounting. Its spectra were very nonstationary, and the correlation between frequency and beam current was small, although the nonstationary nature of the spectra made reliable quantitative estimates of the correlation impossible because the measurements were made sequentially. The tube was operated while bolted to a heat sink cooled with ice water. The frequency noise spectrum under the best operating conditions is shown in Figure 13. This tube was unusual, not only because of its high-power output, but also because it produced severe frequency modulation internally, which was not coherent for about an hour during its warmup. This frequency noise would appear and disappear suddenly, appeared Gaussian when viewed on an oscilloscope, and was not accompanied by any noise or other changes in beam current. Its appearance and disap-

pearance would be accompanied by jumps in frequency of about 2 Mc/s, up and down respectively. The spectrum of this frequency noise is shown in Figure 14. Several other tubes could not be measured at all, because they produced large amounts of coherent frequency modulation; this is the only tube that had an intermittent large-magnitude spurious modulation of a noisy nature.

The data presented in Figures 10, 13, and 14 were taken with the receiver using diode detectors, the data in other figures with the superheterodyne receiver.

COMPARISON WITH MEASUREMENTS AT 30 MC/S

One can expect the spectrum of the frequency modulation resulting from injected beam noise near the signal frequency to be more or less white. Using measurements made at 30 Mc/s away from the carrier, we can estimate the frequency noise near the carrier resulting from beam noise near the carrier. We can estimate by this method what the frequency noise spectrum in the top band should be if it were due entirely to beam noise at the signal frequency. For a QK610 with the carrier shifted 90°, at a power output of 100 mw, we get $\phi_{FM} = 1100$ in the top band. This was interpreted as an upper bound because we were operating here at more than 100 mw output and because this contribution to the spectrum decreased slowly with increasing output power. Thus this source accounted for much of the noise in the higher bands, which was more or less white, and suggested that, at least in the QK610, there was little to be expected between 30 kc/s and 30 Mc/s away from the carrier except white frequency noise and amplitude noise. If we extrapolate inwards in frequency, assuming white AM noise also, we would get a mean-square amplitude-modulation index in the

top band of 10^{-13}, while the mean-square modulation index produced in a signal by the flicker noise in the crystal is about 10^{-10} per half-octave band, whether the crystal is used as a diode detector or a mixer, at least so we observed below 34 kc/s. Thus, in order to be detectable as amplitude noise on a carrier at these low modulating frequencies, a noise source would have to be extraordinarily large, and our inability to detect any amplitude noise was not unexpected. Evaluated in this light, the QK610 is very close to ideal, and spurious low-frequency noise sources such as ions appear to be remarkably well controlled; in fact, there might well be provision for fields to remove ions transversely from the interaction region in this tube.

Rather remarkable in the various tubes is the low-pass weighted components, particularly in the backward-wave oscillators. Except for those components positively identified with power supply frequencies, the cut-off frequencies in the weighting suggests strongly that ions are a significant noise source, this being supported by the behavior of the tubes during warmup.

THEORETICAL ANALYSIS

FREQUENCY NOISE SPECTRUM DUE TO INDEPENDENT IONS

We can estimate the spectrum of the frequency modulation produced by ions if the following conditions are assumed: (1) the ions move independently of each other only in the fields of the average space-charge potential depression of the electron beam; (2) the ions are produced as independent samples of a Boltzman gas and leave only at the ends of the interaction region; (3) the axial motion of the ions is determined solely by that of the gas atom before ionization, and (4) the ions produce only a small perturbation of the beam dynamics, the effect of this perturbation of the ions being neglected. All these conditions can be approached as the vacuum becomes good; when the vacuum is poor one or more of these conditions is not met and so-called ion oscillations might be produced. Since good design practice requires satisfying these conditions, a simple analysis is of value in spite of the restrictive assumptions.

It is necessary at the outset to consider whether momentum transfer between an ion and the passing electrons will be significant. If we suppose an ion is located at the origin and an electron passes with closest approach distance d, then if the transverse motion can be treated as a small perturbation,

$$m\ddot{y} = \frac{-e^2 d}{4\pi \epsilon_o (z^2 + d^2)^{3/2}} \quad ,$$

where y is the small transverse deflection of the electron, and the ion is considered to remain fixed because of its relatively greater mass. We can consider the trajectory alone by using the relation.

$$\ddot{y} = \frac{\partial^2 y}{\partial z^2} v_o^2 = \frac{\partial^2 y}{\partial z^2} \frac{2eE_o}{m} = \frac{2eE_o}{m} y'' \quad ,$$

which gives

$$y'' = \frac{-ed}{8\pi\epsilon_o E_o (z^2 + d^2)^{3/2}} \quad .$$

This can be immediately integrated to give

$$y' = \frac{-e}{4\pi\epsilon_o E_o d} \quad ,$$

or a net transverse velocity of

$$\dot{y} = \frac{-e^{3/2}}{\pi\epsilon_o d(8mE_o)^{1/2}} \quad .$$

It is interesting to compare this in order of magnitude with the transverse thermal velocities in the beam, where

$$\dot{y} \approx \sqrt{\frac{kT}{m}} \qquad \text{or} \qquad y' \approx \sqrt{\frac{kT}{2eE_o}} \quad ,$$

and the electron must come within

$$d \approx \frac{7 \times 10^{-9}}{\sqrt{E_o}} \text{ meters} \quad ,$$

(where E_o is in volts) of the ion to receive a comparable additional velocity. We will ignore such coulomb transverse deflections of electrons as being of too small a magnitude compared with quantum effects. Because of its greater mass, the momentum of the ion will be changed relatively little

by such coulomb interactions.

We now consider the expected total "energy" spectrum of a single ion formed from an ideal gas in the region under consideration. This will be converted to a "power" spectrum by multiplying by the mean number of ions produced per second, but the single event will be discussed first, to permit the greatest flexibility in the physical interpretation.

Suppose that the amount of perturbation of the frequency of the oscillator is known as a position of the ion's position, $g(z)$. This function will be zero outside the interval 0 to A , where A equals $2d$ if ions are removed at one end of the beam only, or A equals d if ions are removed at both ends. It will be assumed that the ion has the probability functions in its axial motion of an ideal gas, where we can use

$$dP_{z_o} = \frac{1}{A}\, dz_o \quad ,$$

if $0 < z_o < A$, and

$$dP_v = \left(\frac{M}{2\pi kT}\right)^{\frac{1}{2}} e^{-(Mv^2/2kT)}\, dv$$

for all v , where we suppose that the ion was formed at $t = 0$, $z = z_o$ with the velocity v without loss of generality. Since when $A = 2d$ then $g(z) = g(A - z)$, and the velocity distribution is even, expressing the probabilities in this form is still quite general. Here we can assume that g is bounded, of bounded variation, and is zero outside the interval from 0 to A . For the total "energy" spectrum, the autocorrelation function, if $v > 0$, is, of the form,

$$C_+(v,\ z_o,\ \tau) = \int_0^{\frac{A - z_o - \tau}{v}} g(vt + z_o)\, g(vt + v\tau + z_o)\, dt \quad ;$$

if $v < 0$, then

$$C_-(v,\ z_o,\ \tau) = \int_{-\tau}^{\frac{-z_o}{v}} g(vt + z_o)\ g(vt - v\tau + z_o)\ dt \quad .$$

We must remember that autocorrelation functions are even in the lag time, and that $g[v(t + \tau) + z_o]$ is zero if $(t + \tau)$ is negative, because the ion has not yet been formed. We use the single-ended cosine transform, so it is necessary to consider only $\tau \geq 0$, but this even property will have to be used anyway. If we define $U = vt$, and $W = |v|\,\tau$, we then have

$$C_+(v,\ z_o,\ \tau) = \frac{1}{v} \int_0^{A-W-z_o} g(U + z_o)\ g(U + W + z_o)\ dU$$

$$C_-(v,\ z_o,\ \tau) = \frac{1}{|v|} \int_{-z_o}^{-W} g(U + z_o)\ g(U + W + z_o)\ dU \quad ,$$

where, as before each of these autocorrelation functions is even in τ or W . If the probability density in v is folded back on itself so that we need consider only $v > 0$, then the expected energy spectrum is

$$S_e(f) = \left(\frac{M}{2\pi kT}\right)^{\frac{1}{2}} \frac{2}{A} \int_0^{\infty} \int_0^{A} \int_0^{A/v} e^{-(Mv^2/skT)} \cos(2\pi f\tau)(C_- + C_+)\ d\tau dz_o\, dv \quad .$$

This expression has so far been considered as a multiple integral. The orders of integration can be interchanged between τ and z_o since both integrals converge absolutely. In the following derivation, changes of vari-

ables are introduced which preclude interpreting the expression as a multiple integral and require treatment as an iterated integral and preventing additional changes in the order of integration. Then,

$$S_e(f) = \frac{2}{A}\left(\frac{M}{2\pi kT}\right)^{\frac{1}{2}} \int_0^{\infty} \int_0^{A/v} e^{-(Mv^2/2kT)} \cos(2\pi f\tau)\, D(W)\, d\tau\, \frac{dv}{v} \quad ,$$

where

$$D(W) = \int_0^{A-W} \left[\int_0^{A-W-z_o} g(U+z_o)\, g(U+W+z_o)\, dU + \int_{-z_o}^{-W} g(U+z_o)\, g(U+W+z_o)\, dU \right] dz_o \quad ,$$

and the region of integration in the U, z_o plane giving $D(W)$ is shown in Figure 15. If we make the change of variable $y = U + z_o$ we can combine the two regions of integration and evaluate to

$$D(W) = (A-W) \int_0^{A-W} g(y)\, g(y+W)\, dy \quad ,$$

which is rather convenient. Now

$$S_e(f) = \frac{2}{A}\left(\frac{M}{2\pi kT}\right)^{\frac{1}{2}} \int_0^{\infty} e^{-(Mf2/2kT)} \int_0^{A/v} \cos(2\pi f\tau)\, D(W)\, d\tau\, \frac{dv}{v} \quad ,$$

and if we substitute $\theta = f/v$, $dv = -fd\theta/\theta^2$, $d\tau = dW/v$, then we get

$$S_e(f) = \frac{2}{fA}\left(\frac{M}{2\pi kT}\right)^{\frac{1}{2}} \int_0^{\infty} e^{-(Mf^2/2kT\theta^2)} \int_0^{A} \cos(2\pi\theta W)\, D(W)\, dW\, d\theta \quad .$$

As a numerical example, suppose g is unity, except where it has

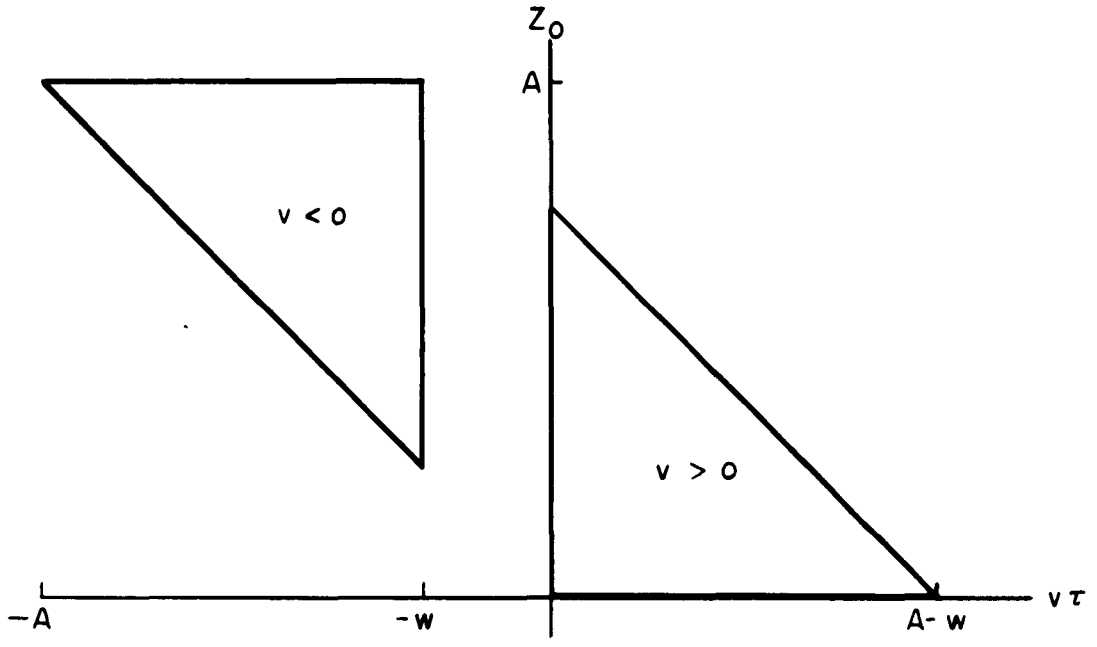

Figure 15. Region in $(v\tau), z_o$ Plane That Contributes to D(W).

already been required to be zero; this would represent a two-cavity klystron oscillator or a two-cavity klystron amplifier (phase noise) for example. Then we can observe directly from Figure 15 that

$$[D(W)] = (A - W)^2 \quad ,$$

so that

$$\int_0^A \cos(2\pi\theta W)(A-W)^2 dW = \frac{A^2}{2\pi\theta} \int_0^{2\pi\theta A} \cos\phi \left(1 - \frac{\phi}{2\pi\theta A}\right)^2 d\phi = \frac{A}{2\pi^2\theta^2}\left[1 - \frac{\sin(2\pi\theta A)}{2\pi\theta A}\right] .$$

It remains only to evaluate

$$S_e(f) = \frac{1}{\pi^2 f}\left(\frac{M}{2\pi kT}\right)^{\frac{1}{2}} \int_0^{\infty} e^{-(Mf^2/2kT\theta^2)}\left[1 - \frac{\sin(2\pi A\theta)}{2\pi A\theta}\right] \frac{d\theta}{\theta^2} \quad .$$

If we substitute $\omega = 2\pi A\theta$ and $\mu = 2\pi Af\sqrt{M/2kT}$ we get the integral with all variables in dimensionless form,

$$S_e(f) = \frac{4A^2}{\mu\sqrt{\pi}}\left(\frac{M}{2kT}\right)\int_0^\infty e^{-(\mu^2/\omega^2)}\left[1 - \frac{\sin\omega}{\omega}\right]\frac{d\omega}{\omega^2} \quad .$$

If we substitute $s = \omega^{-1}$, we get

$$\frac{kT\sqrt{\pi}}{2A^2M}\, S_e(f) \doteq \frac{1}{\mu}\int_0^\infty e^{-\mu^2 s^2}\left[1 - s\,\sin(s^{-1})\right] ds \quad ,$$

where if μ is large, that is, greater than 4 or so, one can approximate

$$\frac{kT\sqrt{\pi}}{2A^2M}\, S_e(f) \cong \frac{1}{\mu}\int_0^\infty e^{-\mu^2 s^2}\, ds \cong \frac{\sqrt{\pi}}{2\mu^2} \quad . \tag{1}$$

Using the integral with respect to ω, when μ is small, one can approximate

$$\frac{kT\sqrt{\pi}}{2A^2M}\, S_e(f) \cong \frac{1}{\mu}\left[\int_0^\infty \left(1 - \frac{\sin(\omega)}{\omega}\right)\frac{d\omega}{\omega^2} - \frac{\mu}{6}\int_0^\infty \left(1 - e^{-x^{-2}}\right) dx\right] \quad .$$

When the last integral is evaluated numerically, the last term is -.2410. Dividing the interval of the first integral at 2 and evaluating 0 to 2 numerically and the rest algebraically finds its value at 0.8025, so that

$$\frac{kT\sqrt{\pi}}{2A^2M}\, S_e(f) \cong \frac{0.8025}{\mu} - .2410 \quad , \tag{2}$$

where the approximation should still be useful up to $\mu = 1$. These two asymptotes as expressed on the right-hand side of these two equations are plotted

in Figure 16, where the vertical co-ordinate is the mean-square value per fraction bandwidth to permit qualitative comparison with the experimental results. The intermediate point was computed numerically. If A equals 1 cm, T equals 300° K, unity μ corresponds to 6690 cps for a N_2^+ ion or to 25 kc/s for a H_2^+ ion.

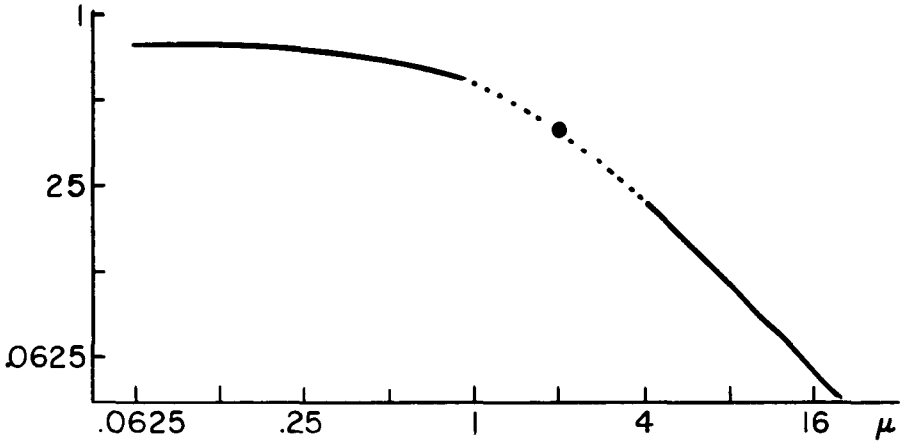

Figure 16. Plot of Equations (1) and (2).

We now have an expression for the "total energy" spectrum of a single event under the assumptions of unity average perturbation of the frequency by the ion. The ion can be considered as a more or less localized perturbation of the beam voltage, the average value of which can be calculated. The square of this value can be applied to the preceding result as a multiplicative factor whose value is specified by theoretical considerations, provided we maintain the constraint,

$$d = \int_0^d g(z)\ dz \quad ,$$

which preserves the interpretation that the variable being described is the equivalent virtual noise in the beam voltage. The total energy spectrum can be converted to a conventional "power" spectrum by multiplying by the average number of ions produced per second, giving a result which has the dimensions of (volts^2 second). This construction removes the tuning rate from the problem and permits more direct comparison of different situations as far as ion noise is concerned. Implicit in this is the assumption that localized small perturbations of the beam voltage can be superimposed to yield the net tuning rate. Now consider the jump in the axial motion of a radially thin, hollow, cylindrical beam of radius b, concentric with a drift tube of radius a and produced by an ion of charge q at $z = 0$, $r = h$, $\phi = \phi_o$. From Smythe's[1] Equation 5.298 (4) we get an expansion of the potential of the ion as

$$V(r, \phi, z) = \frac{q}{2\pi\epsilon_o a^2} \sum_{i=1}^{\infty} \sum_{j=0}^{\infty} \left(2 - \delta_j^o\right) e^{-u_i |z|} \frac{J_j(u_i b) J_j(u_i h) \cos\left[j(\phi - \phi_o)\right]}{u_i J_{j+1}^2 (u_i a)} ,$$

where $\delta_j^o = 1$ if $j = 0$, and $\delta_j^o = 0$ otherwise, and u_i is defined by $J_j(u_i a) = 0$. We are going to assume that the radio-frequency dynamics of the beam are axially symmetric. We can integrate the motion in the z direction under the assumptions that the perturbation is short enough for ballistic dynamics to be valid and that the signal is small, and then we can average the net motion over the beam. We average over the beam first by dropping terms depending on ϕ, leaving

$$V = \frac{q}{2\pi\epsilon_o a^2} \sum_{i=1}^{\infty} e^{-u_i |z|} \frac{J_o(u_i b)\, J_o(u_i h)}{u_i J_1^2 (u_i z)} .$$

In the light of the smallness of the transverse momentum due to interactions, we can integrate the axial motion by using

$$z = \sqrt{\frac{2e(V + E_o)}{m}} \approx \sqrt{\frac{2eE_o}{m}} \left(1 + \frac{V}{2E_o}\right) ,$$

where $z = z_o + \Delta z$, and we have assumed $V << E_o$, the nominal beam voltage, and e is used as a positive number. Then we can integrate the z motion, getting

$$\frac{d\Delta z}{dt} = \sqrt{\frac{2eE_o}{m}} \frac{V}{2E_o} , \quad \Delta z = \int_{-\infty}^{\infty} \frac{V}{2E_o} dz = \frac{q}{2\pi e_o E_o} \sum_{i=1}^{\infty} \frac{J_o(u_i b) j_o(u_i h)}{(u_i a)^2 J_1^2(u_i a)} ;$$

or by defining $X = b/a$ and $Y = h/a$, we can simplify notation by writing

$$\Delta z = \frac{q}{2\pi e_o E_o} \sum_{n=1}^{\infty} \frac{J_o(\lambda_n X) J_o(\lambda_n Y)}{\lambda_n^2 J_1^2(\lambda_n)} = \frac{q W(X, Y)}{2\pi e_o E_o} . \qquad (3)$$

It was decided after tabulating some partial sums of $W(X, Y)$ that

$$W = -1/2 \ln (\text{max of } X \text{ or } Y) ,$$

as can be verified by expanding the right-hand side as Fourier-Bessel sum with X as the variable, and Y as a parameter. By Watson's[2] Equation 18.24 the expansion must exist and be unique, and by his Equation 18.1(2),

$$W(X, Y) = \sum_{n=1}^{\infty} a_n J_o(\lambda_n x) ,$$

where

$$a_n = \frac{-1}{J_1^2(\lambda_n)} \left\{ \int_0^Y X \ln Y \, J_o(\lambda_n X) \, dX + \int_Y^1 X \ln X \, J_o(\lambda_n X) \, dx \right\} \quad ;$$

or defining $u = \lambda_n X$

$$a_n = \frac{-1}{\lambda_n^2 J_1^2(\lambda_n)} \left\{ \ln Y \int_0^{\lambda_n Y} u J_o(u) \, du + \int_{\lambda_n Y}^{\lambda_n} u(\ln u - \ln \lambda_n) J_o(u) \, du \right\} \quad .$$

Using Watson's[2] Equation 5.1(1), we get

$$a_n = \frac{-1}{\lambda_n^2 J_1^2(\lambda_n)} \left\{ \left[\ln Y + \ln(\lambda_n) \right] \lambda_n Y J_1(\lambda_n Y) - \lambda_n J_1(\lambda_n) + \int_{\lambda_n Y}^{\lambda_n} \left[(u) \ln(u) \right] J_o(u) \, du \right\}$$

and integrating the last term by parts gives, after collecting terms,

$$a_n = \frac{J_o(\lambda_n Y)}{\lambda_n^2 J_1^2(\lambda_n)} \quad .$$

Thus under our assumptions (essentially those of good vacuum and small radio-frequency signal), the position of the ion inside a hollow beam does not influence its net effect on the axial motion of the beam.

Note that the average space-charge potential depression of a thin hollow beam effectively confines the ions to the interior of the beam, where their exact position is not important in our model.

We can convert the result of the perturbation of the beam dynamics to an equivalent change of beam voltage by consideration of the transit time t:

$$\Delta t = \frac{\Delta z}{v_o} \quad ,$$

whereas for the d-c beam parameters,

$$t = \frac{d}{v_o} \quad , \qquad \Delta t = \frac{-d\,\Delta v_o}{v_o^2} \quad ,$$

where d is the maximum length of the beam of interest here, so

$$\Delta v_o = \frac{v_o^2\,\Delta z}{-d\,v_o} \quad ,$$

but

$$2eE_o = m\,v_o^2 \quad ;$$

so

$$2e\Delta E_o = 2mv_o\,\Delta v_o$$

and

$$\Delta E_o = \left(\frac{mv_o}{e}\right)\left(\frac{v_o\,\Delta z}{-d}\right) \quad ,$$

or

$$\Delta E_o = \frac{mv_o^2}{-d}\,\Delta z = \frac{-2E_o}{d}\,\Delta z \quad .$$

Substituting in Equation (3) gives

$$\Delta E_o = \frac{e\,\ln(X)}{2\pi e_o d} \quad , \tag{4}$$

where now only singly charged ions are considered and still

$$X = \frac{\text{beam radius}}{\text{drift tube radius}} \quad .$$

The parameter N can be estimated from the results of experimental studies in the field of plasma physics. Brown[3] gives in his Figure 4.21 the "probability of ionization" for some gases of interest, where

$$P_i = \frac{\text{number of ions produced}}{\text{(electron) (cm path length)(mm Hg pressure)}}$$

at $T = 0^\circ C$. We thus have

$$N = \frac{P_i I_o dp}{e} \quad ,$$

where p is the pressure in mm Hg and I_o is the d-c beam current.

All the assumptions made in the preceding discussion would be invalid if the ion space charge is appreciable compared with the electron space charge; therefore this must be checked. If we consider a 625-volt beam, $v_e = c/20$, and if we assume the ions move about the speed of sound, say 300 m/s, then

$$\frac{q_i}{q_e} = \frac{N_i v_e}{N_e v_i} = 5 \times 10^4 \; P_i A p \ll 1 \quad .$$

For a 625-volt beam and the gases N_2, O_2, A, NO, and CO, we have $P_i \approx 5$ so

$$Ap \ll 4 \times 10^{-6} \quad .$$

Note that the length A is in centimeters and the pressure p in mm of Hg. If this inequality is not satisfied, the beam is more or less ion focused and our analysis is not valid. As P_i varies inversely with v_e above elec-

tron energies of 100 of 200 volts, this requirement is independent of beam current or voltage in this range.

The behavior of light gases differs in that not only is M less, but P_i is somewhat less also. Using the experimental results collected by Brown, for hydrogen we get $P_i \approx 0.3$ at 500 volts and

$$Ap << 3 \times 10^{-4} \quad ,$$

while for helium we find $P_i \approx 0.8$ at 500 volts and

$$Ap << 6 \times 10^{-5} \quad .$$

Thus the presence of the heavy bulky gases will be most likely to invalidate our simplifying assumptions.

It should be kept in mind that if a mean rate of ion formation is not properly defined; i.e., if the averaging process giving the variance of the estimates of N is only semi-convergent as the averaging duration is increased, the noise spectrum will be nonstationary.

Before using these results to compute the final power spectrum, we make the changes of variables,

$$\phi = 2\pi\theta, \qquad \lambda = 2\pi f \sqrt{\frac{M}{2kT}}$$

which gives

$$S_e(f) = \frac{M}{kTA\lambda\sqrt{\pi}} \int_0^{\infty} e^{-\lambda^2\phi^{-2}} \int_0^{A} \cos(\phi W)\, dW d\phi \quad .$$

Using the values of ΔE and N given previously gives the power spectrum,

$$S_p(f) = \left[\frac{e\ln(X)}{2\pi e_o d}\right]^2 \left[\frac{P_i I_o p d}{e}\right] \left[\frac{M}{kTA\lambda\sqrt{\pi}}\right] \int_0^{\infty} e^{-\lambda^2\phi^{-2}} \int_0^{A} \cos(\phi W)\, D(W)\, dW d\phi \quad . \tag{5}$$

Note that by virtue of the simplifying assumptions, everything is determined by other known theoretical considerations except $g(z)$, and the effect of various choices of g on the final spectrum is considerably smoothed by the integrations. The particular physical device considered also determines d and A, but these are physical distances that can be measured with a ruler if necessary.

Now we can consider some choices of g that are more plausible for backward-wave oscillators in the frequency range used for the experimental study. If z is in centimeters, one possible function is

$$g_1(z) = \frac{5\pi}{4} \cos\left[\tfrac{1}{2}\pi(z-2)\right] \qquad 1 < z < 3$$

$$= 0 \qquad \text{otherwise} \quad ,$$

and $A = d = 5$ centimeters; then

$$D_1(W) = (5-W)\frac{25\pi^2}{16} \int_1^{3-W} \cos\left[\tfrac{1}{2}\pi(z-2)\right] \cos\left[\tfrac{1}{2}\pi(z+W-2)\right] dz$$

$$= (5-W)\frac{25\pi^2}{32} \int_1^{3-W} \left\{\cos\left[\pi(z-2+\tfrac{1}{2}W)\right] + \cos(\tfrac{1}{2}\pi W)\right\} dz \quad .$$

Let $y = z - 2 + \frac{1}{2}W$, then

$$D_1(W) = \frac{25\pi^2(5-W)}{16} \int_0^{1-\frac{1}{2}W} \left[\cos(\pi y) + \cos\left(\tfrac{1}{2}\pi W\right)\right] dy$$

$$= \frac{25\pi^2(5-W)}{16} \left[\frac{1}{\pi} \sin\left(\tfrac{1}{2}\pi W\right) + \left(1-\tfrac{1}{2}W\right)\cos\left(\tfrac{1}{2}\pi W\right)\right] \quad ,$$

where W is in centimeters. This equation is plotted in Figure 17 as the solid line. If we attempt to approximate this curve with a function more convenient for calculating the remaining integrals, we get the dotted line as the Gaussian curve providing the best second-order fit at W = 0.

For comparison, consider

$$g_2(z) = \frac{5\pi}{2} e^{-\left(\frac{\pi(z-2)}{2}\right)^2} \quad ,$$

with A = d = 5 centimeters. Both g_1 and g_2 satisfy the constraint

$$\int_0^d g(z)dz \cong d \quad ,$$

and g_2 has the "autocorrelation function,"

$$D_2(W) = \frac{25(5-W)\sqrt{\pi}}{2\sqrt{2}} e^{-(\pi^2 W^2/8)} \quad ,$$

where the exponential factor is just the Gaussian fit in Figure 17 shown as the dotted line, and the numerical constants are

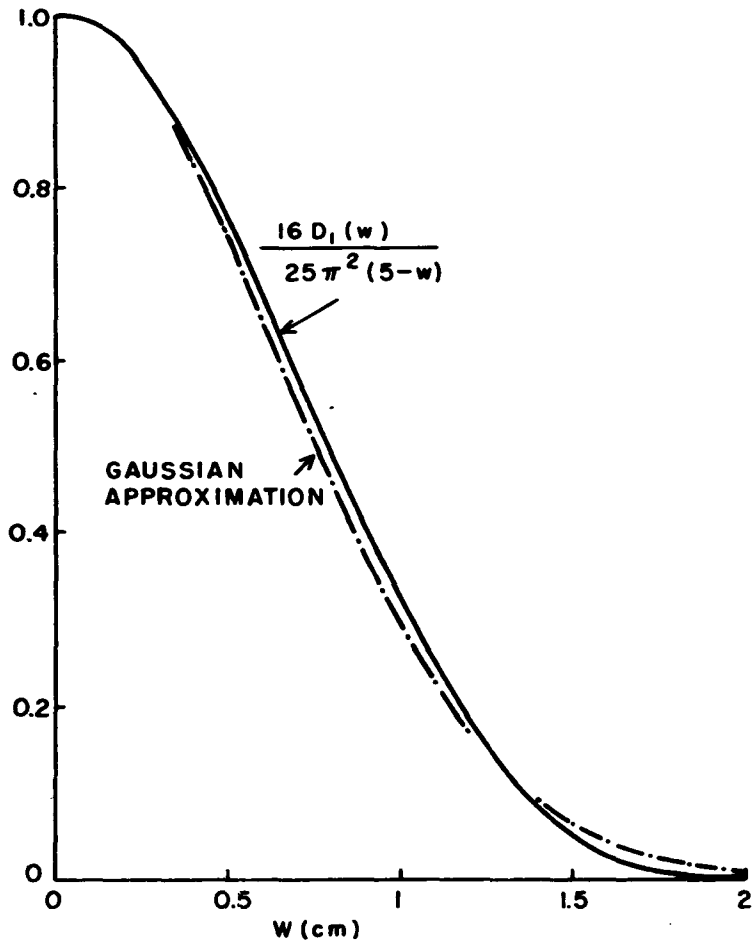

Figure 17. $D_1(W)$ and Gaussian Approximation.

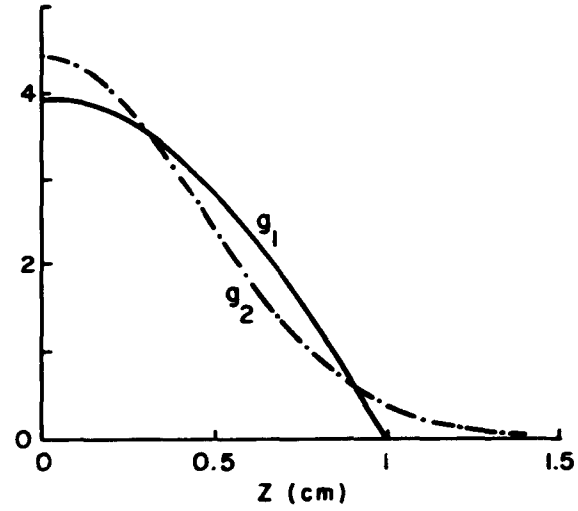

Figure 18. Weighting Functions g_1 and g_2.

$$\frac{25\sqrt{\pi}}{2\sqrt{2}} = 15.66 , \qquad \frac{25\pi^2}{16} = 15.42 ,$$

so the approximation is rather good. We will use $D_2(W)$ to compute the spectrum for both of these weighting functions. The two g functions are plotted in Figure 18 to illustrate how rather different choices of g can give similar D functions. In order to exploit the properties of $D_2(W)$ we will let the upper limit of the integral in W be infinite, which introduces little error and much convenience.

We desire to compute

$$S_p(f) = K \int_0^\infty e^{-\lambda^2\phi^{-2}} \int_0^\infty \cos(\phi W)(5-W)\, e^{-(\pi^2 W^2/8)}\, dW d\phi ,$$

where

$$K = \frac{25}{2\sqrt{2}} \left[\frac{e\ \ln(X)}{2\pi e_o d}\right]^2 \left[\frac{P_i I_o p dM}{ekTA\lambda}\right] ,$$

and since λ is included in K, then the remainder of the expression is in power per unit fractional bandwidth. Consider

$$F(\phi) = \int_0^\infty (5-W) \cos(\phi W)\, e^{-(\pi^2 W^2/8)}\, dW ;$$

or, evaluating the first term,

$$F(\phi) = \frac{5}{2}\sqrt{\frac{8}{\pi}}\, e^{-(2\phi^2/\pi^2)} - \mathrm{Re} \int_0^\infty W\, e^{-(\pi^2 W^2/8 + j\phi W)}\, dW ;$$

or completing the square,

$$F(\phi) = \frac{5\sqrt{2}}{\sqrt{\pi}} e^{-(2\phi^2/\pi^2)} - e^{-(2\phi^2/\pi^2)} \operatorname{Re} \int_0^\infty W e^{-(\pi W/8 + j\phi\sqrt{8}/2\pi)^2} dW \quad .$$

Now let

$$z = \frac{\pi W}{\sqrt{8}} + \frac{j\phi\sqrt{2}}{\pi} \quad , \qquad dW = \frac{\sqrt{8}}{\pi} dz \quad , \qquad W = \frac{z\sqrt{8}}{\pi} - \frac{j4\phi}{\pi^2} \quad ,$$

then

$$F(\phi) = \frac{5\sqrt{2}}{\sqrt{\pi}} e^{-(2\phi^2/\pi^2)} - e^{-(2\phi^2/\pi^2)} \operatorname{Re} \int_{j\phi\sqrt{2}/\pi}^\infty \left[\frac{8z}{\pi^2} - \frac{j\phi 8\sqrt{2}}{\pi^3}\right] e^{-z^2} dz \quad ;$$

or deforming the contour through the origin,

$$F(\phi) = \frac{5\sqrt{2}}{\sqrt{\pi}} e^{-(2\phi^2/\pi^2)} - e^{-(2\phi^2/\pi^2)} \left\{ \frac{4}{\pi^2} \int_0^\infty 2z\, e^{-z^2} dz \right.$$

$$\left. + \operatorname{Re} \int_{-j\phi\sqrt{2}/\pi}^0 \left(\frac{8z}{\pi^2} - \frac{j\phi 8\sqrt{2}}{\pi^3}\right) e^{-z^2} dz \right\} \quad .$$

If we now substitute $z = jy$, we get

$$F(\phi) = \frac{5\sqrt{2}}{\sqrt{\pi}} e^{-(2\phi^2/\pi^2)} - e^{-(2\phi^2/\pi^2)} \left\{ \frac{4}{\pi^2} + \int_{\phi\sqrt{2}/\pi}^0 \left(\frac{\phi 8\sqrt{2}}{\pi^3} - \frac{8y}{\pi^2}\right) e^{y^2} dy \right\} \quad .$$

Calculating the last integral and interchanging upper and lower limits on the first gives

$$F(\phi) = \frac{5\sqrt{2}}{\sqrt{\pi}} e^{-(2\phi^2/\pi^2)} - \frac{4}{\pi^2} + \frac{\phi 8\sqrt{2}}{\pi^3} \int_0^{\phi\sqrt{2}/\pi} e^{t^2} dt \quad .$$

This last integral is tabulated on page 32 of Jahnke & Emde[4] for $0 < \frac{\phi\sqrt{2}}{\pi} < 2$. For larger arguments, an asymptotic expansion of this integral is needed. Consider

$$\int_0^x e^{t^2} dt = e^{x^2} \int_{-x}^{0} e^{(2xt + t^2)} dt = e^{x^2} \int_0^x e^{-2xt} e^{t^2} dt = \frac{e^{x^2}}{2x} \int_0^{2x^2} e^{-y} e^{+(y/2x)^2} dy .$$

If x is large, this last integral can be approximated by expanding the last exponential in power series and using only the first few terms, interchanging the order of summation and integration, and evaluating each term approximately by making its upper limit infinity. As the available tables cover the variable x only up to 2, this expansion should have optimum accuracy at $x = 2$ if the first four terms are kept, giving

$$\int_0^x e^{t^2} dt \cong \frac{e^{x^2}}{2x} \left[1 + \frac{1}{2x^2} + \frac{3}{4x^4} + \frac{15}{8x^6}\right] .$$

In our application, $x = \phi\sqrt{2}/\pi$, so if $x < 2$, we can use the tables to evaluate

$$F(\phi) = \frac{5\sqrt{2}}{\sqrt{\pi}} e^{-x^2} - \frac{4}{\pi^2} + \frac{8x}{\pi^2} e^{-x^2} \int_0^x e^{t^2} dt ,$$

while if $x > 2$, the asymptotic expansion gives

$$F(\phi) \cong \frac{5\sqrt{2}}{\sqrt{\pi}} e^{-x^2} + \frac{2}{\pi^2} \left(\frac{1}{x^2} + \frac{3}{2x^4} + \frac{15}{4x^6}\right) .$$

At $x = 2$, the two expressions agree within one-half per cent; $F(\phi)$ is plotted in Figure 19.

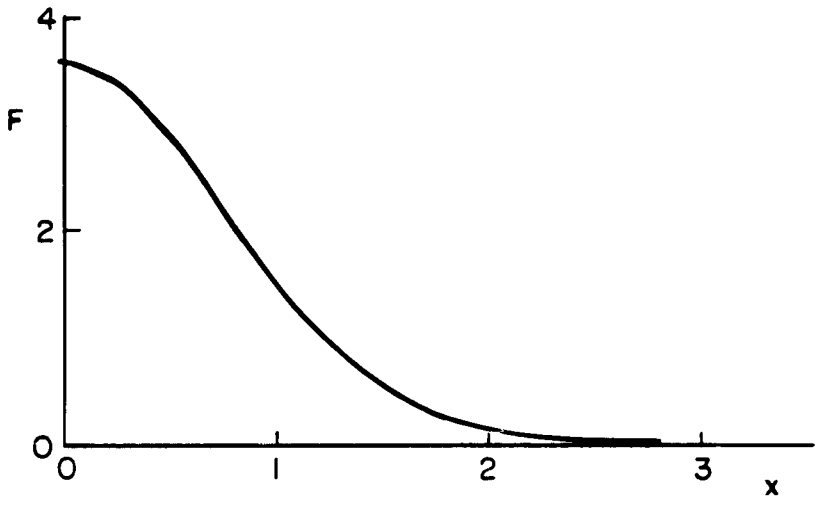

Figure 19. F versus x .

If we now define

$$\gamma = \frac{\sqrt{2}}{\pi}\lambda = 2f\sqrt{\frac{M}{kT}} \quad ,$$

the noise spectrum takes the convenient form,

$$S_p(f) = K' \int_0^\infty e^{-\gamma^2 x^{-2}} F(\phi)dx \quad ,$$

where

$$K' = \frac{25}{2}\left[\frac{e\,\ln(X)}{2\pi e_o d}\right]^2 \left(\frac{P_i I_o p dM}{ekTA\pi\gamma}\right) \quad ;$$

and again the frequency dependence of K' is such that the remainder of the expression is relative noise per fraction bandwidth. Here the first term of F permits part of the integral to be evaluated algebraically, giving

$$\frac{S_p(f)}{K'} = \frac{5}{\sqrt{2}} e^{-2\gamma} + \int_0^\infty e^{-\gamma^2 x^{-2}} F_2(x)\, dx \quad ,$$

where F_2 is merely the rest of the expression for F. If $\gamma > 2$, the asymptotic expansion for F_2 can be used to evaluate this integral, giving

$$\frac{S_p(f)}{K'} = \frac{5}{\sqrt{2}} e^{-2\gamma} + \frac{1}{\pi^{3/2}} \left[\gamma^{-1} + \frac{3}{4}\gamma^{-3} + \frac{45}{16}\gamma^{-5}\right] \quad .$$

In the same manner as above, for small γ, we can approximate

$$\frac{S_p(f)}{K'} = \frac{5}{\sqrt{2}} e^{-2\gamma} -.00316 + .58603\gamma \quad .$$

These two asymptotes with intermediate points computed numerically are shown in Figure 20. Unity γ at 300°K for N_2 ions is 14.7 kc/s, for H_2 ions, 55 kc/s.

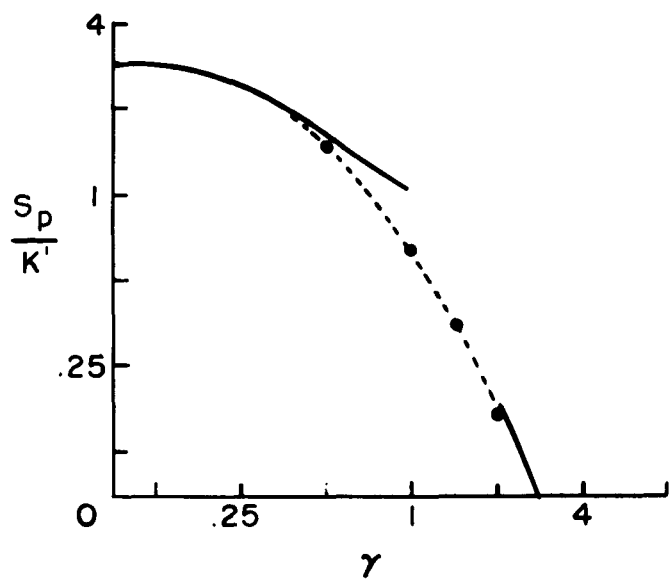

Figure 20. Spectrum for g_2, with d = A = 5 cm.

If we assume that X is 0.82, T = 300°K, p = 10^{-7} mm Hg, we get for N_2 ions

$$K'\gamma = 1.854 \times 10^{-11} \quad ,$$

which is quite compatible with the experimental results shown in Figure 12, for example.

We have so far considered only cases where the ions were removed at both ends of the interaction region. We might represent a backward-wave oscillator with ions removed only at the cathode by

$$g_3(z) = \frac{5\pi}{2} \left\{ e^{-\left[\frac{1}{2}\pi(x-2)\right]^2} + e^{-\left[\frac{1}{2}\pi(z-8)\right]^2} \right\} \quad ,$$

where again

$$\int_0^d g(z)\, dz \approx d, \qquad d = 5\,\text{cm}, \qquad A = 10\,\text{cm} \quad .$$

By separating this into four integrals and comparing each with that giving D_2, we can at once conclude that

$$D_3(W) = \frac{25(10-W)\sqrt{\pi}}{2\sqrt{2}} \left[2e^{-(\pi^2 W^2/8)} + e^{-(\pi^2(W-6)^2/8)} \right] \quad ,$$

where a term containing a factor,

$$e^{-(\pi^2(W+6)^2/8)} \quad ,$$

has been dropped, since only positive W is to be used.

We can proceed using the same notation as with D_2 provided we define

$$F(\phi) = \int_0^\infty \cos(\phi W)(10-W)\left\{2e^{-(\pi^2 W^2/8)} + e^{-\left[\pi^2(W-6)^2/8\right]}\right\} dW$$

$$= \frac{20\sqrt{2}}{\sqrt{\pi}}\, e^{-(2\phi^2/\pi^2)} - 2\int_0^\infty W\cos(\phi W)\, e^{-(\pi^2 W^2/8)}\, dW$$

$$+ \int_{-\infty}^\infty (4-\Omega)\cos\left[\phi(\Omega+6)\right]\, e^{-(\pi^2\Omega^2/8)}\, d\Omega \quad .$$

Since the second term was already dealt with for D_2, it is available in tabular form and can be combined with the others in the next integration. Proceeding with the $d\Omega$ integral, we get

$$F(\phi) = \frac{20\sqrt{2}}{\sqrt{\pi}}\, e^{-(2\phi^2/\pi^2)} - 2F_2(\phi) + 4\cos(6\phi)\int_{-\infty}^\infty \cos(\phi\Omega)\, e^{-(\pi^2\Omega^2/8)}\, d\Omega$$

$$+ \sin(6\phi)\int_{-\infty}^\infty \Omega\sin(\phi\Omega)\, e^{-(\pi^2\Omega^2/8)}\, d\Omega$$

$$= \frac{20\sqrt{2}}{\sqrt{\pi}}\, e^{-(2\phi^2/\pi^2)} + F_2 + \left[\frac{8\sqrt{2}}{\sqrt{\pi}}\,\frac{\phi}{\pi^2}\sin(6\phi)\, e^{-(2\phi^2/\pi^2)}\right]$$

$$+ \left[\frac{8\sqrt{2}}{\sqrt{\pi}}\cos(6\phi)\, e^{-(2\phi^2/\pi^2)}\right] \quad ,$$

where the last three terms will require numerical integration. If we now change variables to x and γ as before, we get

$$\frac{S_p(f)}{K'} = 10\sqrt{2}\, e^{-2\gamma} + 2\int_0^\infty F_2(\phi)\, e^{-\gamma^2 x^{-2}}\, dx + \int_0^\infty \left[\frac{8\sqrt{2}}{\sqrt{\pi}} \cos\left(\frac{6\pi x}{\sqrt{2}}\right) + \frac{8x}{\pi^{3/2}} \sin\left(\frac{6\pi x}{\sqrt{2}}\right)\right] e^{-(x^2 + \gamma^2 x^{-2})}\, dx \quad .$$

The last integral is negligible compared with the first two terms, as was emphasized by the fact that attempts to integrate it numerically gave results of the same order as the error to be expected. In all cases computed, the last term was less than 2 per cent of one of the other two, so it is dropped here, leaving for small γ ,

$$\frac{S_p(f)}{K'} = 14.14213\, e^{-2\gamma} - 0.00632 + 1.17206\gamma$$

and for large γ ,

$$\frac{S_p(f)}{K'} = 14.14213\, e^{-2\gamma} + 0.35917 \left[\gamma^{-1} + \frac{3}{4}\gamma^{-3} + \frac{45}{16}\gamma^{-5}\right] \quad ,$$

which are plotted in Figure 21 together with some intermediate points computed numerically.

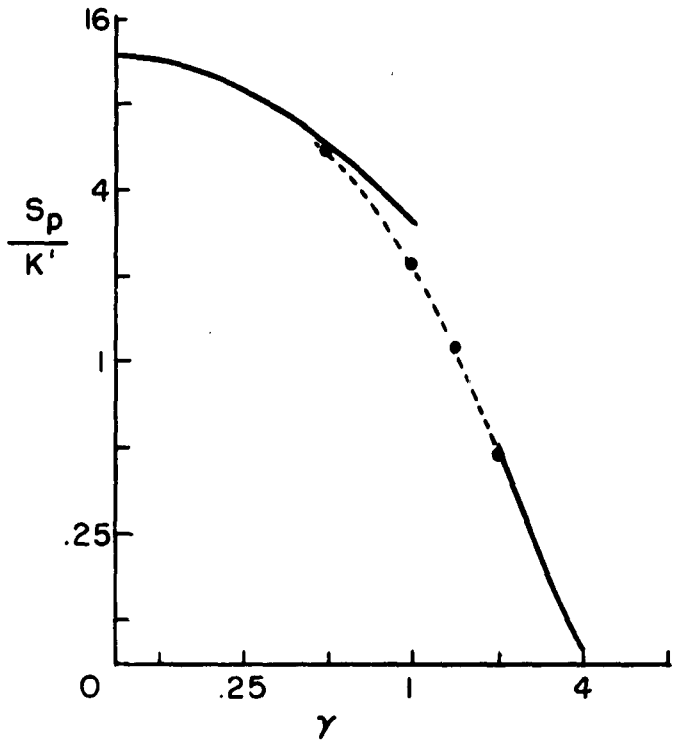

Figure 21. Spectrum for g_3, with 2d = A = 10 cm.

DISCUSSION AND CONCLUSION

It is fairly clear that in the particular VA-161 tubes tested the vacuum was too poor to permit application of the rather simple theory that attributes the noise to independent ions. The QK-610 and 357H appear to have relatively good vacuums, so that this theory may be applicable. In these two tubes the observed frequency noise spectrum is compatible with this theory and with the quality of vacuum that can be reasonably expected in the tubes. It is hoped that controlled experiments with the composition of the vacuum documented can be conducted in the future.

The difficulties with lead leakage encountered indicate that reducing it would be of considerable benefit to users of such tubes, since the noise generated in such leakage is very nonstationary. Problems with spurious, coherent, frequency modulation seem to be relatively common and, together with the leakage, indicate that more emphasis on details of design and processing is perhaps needed. In any case, better vacuum is needed, and perhaps this can be achieved most easily by careful processing and provision for adequate cooling.

REFERENCES

1. W. R. Smythe, Static and Dynamic Electricity, N. Y.: McGraw Hill, 1950.

2. G. N. Watson, Theory of Bessel Functions, Cambridge, Eng.: 1922.

3. S. C. Brown, Basic Data of Plasma Physics, N. Y.: Wiley, 1959

4. E. Jahnke and F. Emde, Tables of Functions, N. Y.: Dover, 1945.

5. R. B. Blackman and J. W. Tukey, The Measurement of Power Spectra, N. Y.: Dover, 1959.

6. A. Erdelyi, Asymptotic Expansions, N. Y.: Dover, 1956.

7. H. B. Dwight, Mathematical Tables, N. Y.: Dover, 1958.